S.I.: INDUCED SEISMICITY AND ITS EFFECTS ON BUILT ENVIRONMENT

Seismic assessment of a lab-tested two-storey unreinforced masonry Dutch terraced house

Rita Esposito[1] · **Francesco Messali[1]** · **Geert J. P. Ravenshorst[2]** · **H. Roel Schipper[1]** · **Jan G. Rots[1]**

Abstract

The exploitation of geo-resources in the northern part of the Netherlands (Groningen region) is triggering shallow earthquakes, rising the need of assessing the current building stock. Being the region not prone to tectonic earthquakes, buildings are designed as wind-resistant systems and have specific characteristics that can limit their seismic performance. In this framework, an extensive research has been carried out on the performance of low-rise unreinforced masonry (URM) buildings at Delft University of Technology. Major attention was focussed on the behaviour of terraced houses, which represent the majority of structures within the URM building stock. In this paper, the case study of a modern Dutch terraced house, built after 1980, made of calcium silicate element masonry and reinforced concrete floors is considered. A quasi-static cyclic test on a full-scale two-storey structure resembling the considered typology is presented. The experimental results are used to evaluate the seismic performance of the structure in the framework of the nonlinear static analyses. A comparative study highlights the importance of the selection of the assessment procedures. Adopting the experimental results as a benchmark, a blind prediction contest revealed a large output variability depending on the adopted analysis method and modelling choices. Consequently, the cross-validation among different analysis methods currently appears the best approach to achieve a more accurate prediction of the structural capacity. The combined experimental and numerical work presented in this paper allows gaining a deeper insight on the evaluation of the seismic performance of Dutch terraced houses.

Keywords Full-scale quasi-static cyclic test · Calcium silicate (CS) element masonry · Dutch terraced house · Seismic assessment · Blind prediction contest

✉ Rita Esposito
r.esposito@tudelft.nl

Extended author information available on the last page of the article

Fig. 1 **a** Typical Dutch terraced houses; **b** prescriptive rules for the design against wind load (NEN 2012)

1 Introduction

In the past decade it has become clear that the exploitation of geo-resources is triggering human-induced shallow earthquakes in the Groningen region, located in the northern part of the Netherlands (van Elk and Doornhof 2017). These earthquakes are characterised by small-magnitude ($M_L < 3.5$) and occur within a depth of approximately 4 km (van Eck et al. 2006). This man-made hazard has progressively become important for the area, especially after the first major event (local magnitude $M_L = 3.6$, peak ground acceleration of 0.08 g) recorded in 2012 in Huizinge (Bourne et al. 2015; Vlek 2018).

The seismic assessment of the unreinforced masonry (URM) building stock becomes a relevant issue especially with focus on low-rise residential buildings (e.g. terraced and detached houses). In the Groningen region, approximately 70% of the building stock is composed of URM buildings, among which terraced houses represent one of the largest typologies. Although many differences can be found from building to building, terraced houses have specific characteristics that can limit their seismic performance. Being an agglomerate of 5 to 10 houses, each terraced house is typically a two-storey masonry building. They are characterised by a narrow floor plan being approximatively 5 m in width and 7–9 m in depth. The inter-storey height varies typically between 2.5 and 2.7 m. The presence of large daylight openings in the facades reduces the loadbearing structure to be composed of slender piers, while orthogonally long transversal walls are used as house-to-house separation walls. The walls are mainly cavity walls having two leaves, with a thickness of 100 mm each, separated by a gap of 60 to 80 mm and connected by steel ties. The masonry types used for the two leaves generally differ: for the inner leaf mainly calcium silicate (CS) brick, block or element masonry is used, while for the outer leaf the use of clay brick masonry is common. The floors are generally made of reinforced concrete; some exceptions are also known where the top floor is in timber. The floors, which can span only between transversal walls, can be continuing for more than a house or spanning only on a single house. Timber roofs having purlins spanning between the transversal walls are generally used.

Being the area not prone to tectonic earthquakes, Dutch terraced houses were not designed accordingly to specific seismic-resistant criteria, while wind load is mainly considered. For optimal sunlight insight the houses, only narrow piers are used in the facades (Fig. 1). A prescriptive rule (NEN 2012), which gives a requirement to the summation of the pier lengths for the whole block, is generally adopted for wind design. To provide structural continuity, the floor slabs between the different houses are connected. The presence of slender piers and the limited connectivity between the structural elements make terraced houses vulnerable to seismic load in particular in the direction parallel to the façade piers.

To evaluate the seismic performance of terraced houses, a quasi-static cyclic test was carried out on a full-scale two-storey specimen resembling a modern terraced house built after 1980. The experiment was part of a multiscale experimental campaign including also tests for the characterisation of the behaviour at component, material and connection level (Damiola et al. 2018; Esposito et al. 2018; Jafari and Esposito 2017; Jafari et al. 2018; Messali et al. 2018a). If care is taken in the selection of an appropriate loading pattern and in the control procedure adopted during the experiment (Calvi et al. 1996), quasi-static tests can represent a good testing method to evaluate the seismic performances of buildings with rigid diaphragm. Although dynamic effect cannot be captured, insights on the progressive damage evolution of the structure and its impact on the global structural behaviour can be studied making the quasi-static test results valuable benchmarks for the validation of analysis methods. In this respects, only few examples of quasi-static tests on full-scale URM structures can be found in literature, such as Aldemir et al. (2017), Yi et al. (2006) and Magenes et al. (1995). Additionally, the presented experiment provides further information on a building typology, typical of the north part of Europe, that has been limitedly studied with respect to seismic performance (Anthoine and Capéran 2008; Degée et al. 2008; Graziotti et al. 2017, 2018; Mayer and Caballero Gonzaléz 2008; Tomassetti et al. 2018).

A global seismic assessment of the studied structures is performed within the framework of nonlinear static analysis considering different assessment procedures. The seismic assessment is performed making use of the newly released Dutch standard NPR 9998:2018 for the assessment of structural safety due to induced seismicity (NEN 2018). Three assessment procedure are compared, namely the capacity spectrum method (CSM), the general N2 method (CEN 2005; Fajfar 1999) and a recent alternative of the N2 method formulation specific for short-period URM structures (Guerrini et al. 2017).

Being nonlinear static analyses commonly used within the engineering practice, the experimental test has been proposed as a benchmark within a blind prediction contest that involved nine engineering consultants (Messali et al. 2018b). Different analysis methods among which finite element, equivalent frame and analytical approaches were adopted. The experimental results proved to be an excellent benchmark for the validation of the analysis methods.

2 Materials and method

The case study presented in this paper refers to modern Dutch terraced houses typically built after 1980 and still largely adopted in nowadays construction practice. Due to the economic prosperity following the second world war, the use of terraced houses in the Netherlands (and north part of Europe) largely increased making this typology the largest part of the URM buildings in the area subjected to induced seismicity.

A full-scale two-storey assemblage representing the inner loadbearing structure of a typical modern Dutch terraced house was tested at Delft University of Technology (Esposito et al. 2018). The specimen consisted of two transversal walls on the west and east side and two identical facades on the north and south side (Fig. 2). Due to limitation of the set-up the width of the assembled structure was limited to 5.4 m, while the length of 5.4 m is in agreement with practice. To imitate the presence of large window openings (Fig. 1a), the facades consisted of two piers having respectively a length of 1.1 m (wide piers P1 and P3) and of 0.6 m (narrow piers P2 and P4). The masonry was
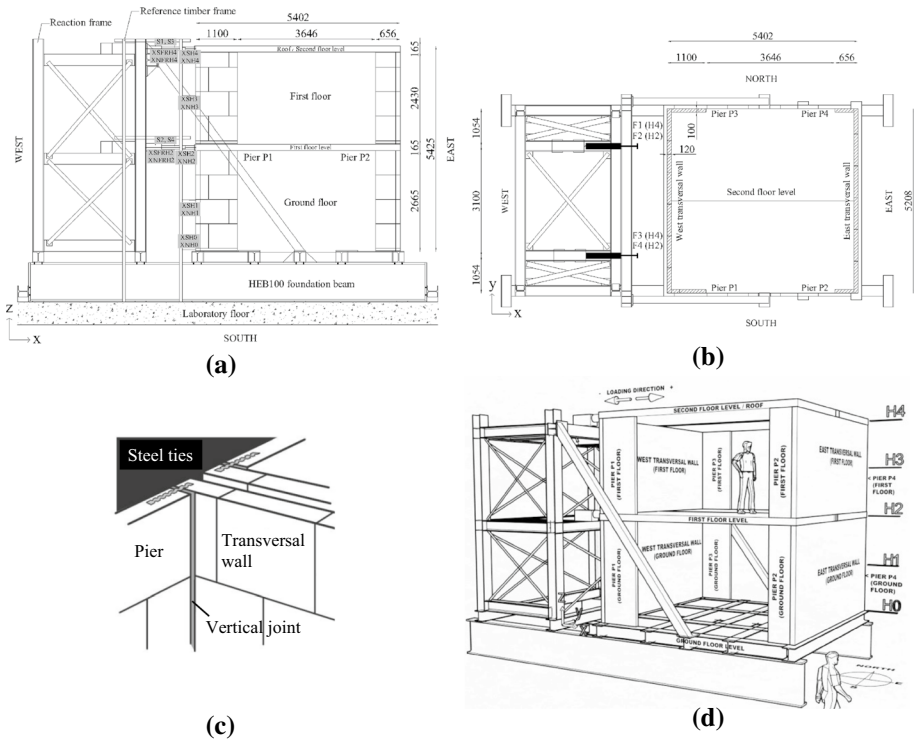
Fig. 2 Specimen and test set-up (dimensions in mm): **a** front view (south side); **b** top view at second floor level; **c** details of wall-to-pier connection; **d** 3D representation

built in stretcher bond using units with a thickness of 100 and 120 mm for the façade piers and the transversal walls, respectively. The length and height of the CS elements were 897 and 643 mm, respectively; these dimensions were tailor made in the factory on the basis of the structure's geometry as commonly done in practice. Thin layer cement-based mortar was used with a joint thickness of 2 and 3 mm for head and bed joints, respectively. To ensure verticality of the wall, a kicker layer made of smaller masonry units was adopted at the bottom of the walls both at the ground and first floor. Due to the large dimensions of the masonry units, the connection between the façade piers and the transversal wall consisted of a thin vertical joint filled with the same mortar. Additionally, steel ties were embedded at every mortar bed joint between transversal walls and piers, with the exception of the first and last mortar joint that connected the masonry with the kicker layer and the floor, respectively (Fig. 2c). The steel ties, having dimension of $300 \times 22 \times 0.7$-mm ($L \times B \times t$), were certified by the producer with a tensile and shear strength of 1260 and 400 N, respectively. Each floor consisted of two separated prefabricated reinforced concrete slabs connected by cast-in-place reinforced concrete dowels, aiming to approach the behaviour of a monolithic floor (Fig. 2b). The thickness of the floor was set to 165 mm to account for additional masses. The floors were one-way spanning between the transversal walls and they were laid up in a mortar bed joint with thickness of 10 mm (general purpose cement-based mortar) on the two transversal walls; the joints between the floor and the piers were filled in a second stage.

Table 1 Material properties of CS element masonry, concrete floor and floor-to-wall connection (Esposito et al. 2016; Jafari and Esposito 2017; Jafari et al. 2018)

Material property	Symbol	Unit	Average	C.o.V.	No. tests	Testing standard
Density	ρ	kg/m³	1824	0.02	22	EN 1015-11 (CEN 1999)
Compressive strength of mortar (thin-layer mortar)	f_m	MPa	16.10	0.09	36	EN 1015-11 (CEN 1999)
Normalised compressive strength of masonry unit	f_b	MPa	19.50	0.16	18	EN 772-1 (CEN 2000)
Compressive strength of masonry perpendicular to the bed joints	f'_m	MPa	13.93	0.07	5	EN 1052-1 (CEN 1998)
Elastic modulus of masonry in the direction perpendicular to bed joints	E	MPa	8557	0.19	6	EN 1052-1 (CEN 1998)
Compressive strength of masonry parallel to the bed joints	$f'_{m,h}$	MPa	9.42	0.17	6	Similar to EN 1052-1 (CEN 1998)
Elastic modulus of masonry in the direction parallel to the bed joints	E_h	MPa	8416	0.17	6	Similar to EN 1052-1 (CEN 1998)
Out-of-plane masonry flexural strength parallel to the bed joint	f_{x1}	MPa	0.58	0.14	5	EN 1052-2 (CEN 2015)
Out-of-plane masonry flexural strength perpendicular to the bed joint	f_{x2}	MPa	0.73	0.04	4	EN 1052-2 (CEN 2015)
Masonry initial shear strength of calcium silicate masonry	f_{v0}	MPa	0.83	–	11	EN 1052-3 (CEN 2002)
Masonry shear friction coefficient of calcium silicate masonry	μ	–	1.48	–	11	EN 1052-3 (CEN 2002)
Cubic compressive strength of concrete	f_{cc}	MPa	74.7	0.02	6	EN 12390-3 (CEN 2009)
Initial shear strength of bed joint between concrete floor and CS element masonry (general purpose mortar)	$f_{v0,cm}$	MPa	0.09	–	9	Similar to EN 1052-3 (CEN 2002)
Shear friction coefficient of bed joint between concrete floor and CS element masonry (general purpose mortar)	μ_{cm}	–	0.52	–	9	Similar to EN 1052-3 (CEN 2002)

Table 1 lists the relevant material properties; for further information the reader can refer to Esposito et al. (2016), Jafari and Esposito (2017) and Jafari et al. (2018).

A quasi-static cyclic test was performed by loading the structure parallel to the façade piers (X-axis in Fig. 2). The structure was built on a stiff foundation and sliding at the base of the structure was suppressed by gluing the first kicker layer to the foundation beams. A steel reaction tower was used as reaction frame. The masonry structure was loaded by four actuators, two per each floor, positioned at approximatively 1.1 m inwards from the facades (Fig. 2b). A displacement was imposed at the second floor level, while a ratio 1:1 was maintained between the forces at the two floor levels (F1 + F3 = F2 + F4) by mechanically coupling the actuators (F1 = F3, F2 = F4). Due to the adopted control system, undesired torsional deformations were prevented at the second floor level, where the same displacement was imposed in the actuators (S1 = S3), and they were limited at the first floor level due to the coupling of the actuators between the floors. The selected force distribution is one of the possible representative loading configuration to account for the seismic action and compatible with the similar mass proportion between the floors. This choice is also supported by the results of a shaking-table test on a similar building that reported an uniform force distribution (Graziotti et al. 2015). The test was performed in 5 phases, which took place in different days; at the beginning of every phase (except the first one) a small cycle with an imposed displacement in the top actuators of ± 0.2 mm and the last cycle of the previous phase were repeated. The load was applied by means of reversed cycles, each of them composed of 3 identical runs. A run is defined as the time needed to apply the maximum positive and negative target displacement starting and ending at zero. The loading rate per each cycle was first imposed to obtain a cycle duration of 15 min until a maximum rate of 1 mm/s was reached and then kept constant. A stiff reference timber frame was adopted as reference to measure the global displacement of the structure. Wire or laser sensors were adopted to measure the displacements along the X- and Y-axis, while potentiometers were used to measure relative displacements (opening and sliding) at wall/pier-to-floor and wall-to-pier connection.

3 Experimental results

The overall behaviour of the assembled structure is shown in Fig. 3 in terms of capacity curve and inter-storey drift. The capacity curve (Fig. 3a) is expressed in terms of base shear force, calculated as the sum of the forces in the actuators, versus the displacement at second floor level, calculated as the average displacement measured with respect to the reference timber frame next to the actuators at floor level (sensors XNH4 and XSH4, Fig. 2). The inter-storey drifts (Fig. 3b) have been calculated considering an inter-storey height of 2669 and 2442 mm for the ground and first floor, respectively. The inter-storey drift is given as a function of the displacement at second floor level calculated for each cycle by averaging the maximum and minimum displacement in each of the three runs.

The global response of the structure is governed by the in-plane behaviour of the façade piers. To highlight this relationship, markers in Fig. 3a show relevant damage levels; each marker is located in correspondence of the minimum and maximum peak value of the cycle in which the corresponding damage occurred.

The first damage occurred at the bottom and top of both the piers and the transversal walls in correspondence of the mortar joints connecting, respectively, the masonry to the kicker layer and the masonry to the concrete floor. This damage, which provides a slight
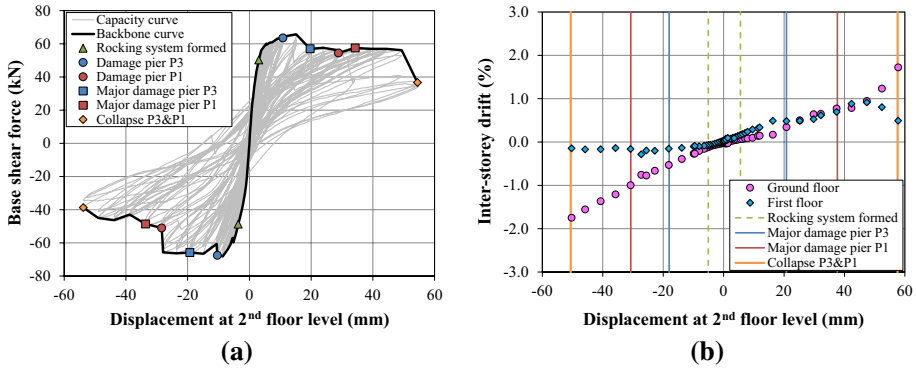
Fig. 3 Overall performance of assembled structure: **a** capacity and backbone curves with indication of cycles at which significant damage occurred; **b** inter-storey drifts

reduction in stiffness and a limited energy dissipation, leads to the formation of a rocking system (green triangular marker in Fig. 3a) in which the piers rotate as rigid members. After the formation of the rocking mechanism, an increase of base shear force was observed. This increase can be explained by the increase in axial force in the piers while deforming, which is accentuated by the presence of a rigid diaphragm. The reinforced concrete floor provided relative strong coupling between the façade piers allowing for a axial force redistribution similar to the one observed in a portal system. An additional contribution to the increase of the axial force on the piers can be also provided by the partial uplift of the transversal walls (flange effect).

After the formation of the rocking system and before the damage in the wide piers, the progressive deformation of the structure triggered cracking and sliding at the vertical joints connecting the piers and the transversal walls. This phenomenon occurred at any connection, but it was predominant for the piers located at ground floor. Although all connections of the pier with the rest of the structure were damaged (top, bottom and vertical joints), a coupled deformation of piers and transversal walls was observed thanks to the presence of steel anchors placed at each bad joint in the connection and to the sliding friction mechanism triggered by the relative vertical displacement between pier and transversal wall. In this configuration, the piers behaved as a rigid block deforming primarily in its plane, but showing also an out-of-plane rotation (Puente et al. 2018). This phenomenon was predominant for the wide piers at ground floor. Furthermore, the damage in the transversal walls localised in their central part with cracking of head and bed joints. This type of damage is compatible with the in-plane deformation of the piers and suggests the presence of a flange effect, despite the limited connection provided by vertical joints.

Subsequently, the damage within the wide piers at the ground floor led to progressive reduction in base shear force and to the increase in energy dissipation. The damage occurred first in the pier P3 located on the north façade and afterwards on pier P1 located on the south façade. For both cases, damage initiates in the top part of the wide piers with sliding over bed joints and opening of head joints (circle markers in Fig. 3a). Afterwards, splitting of the masonry units at the bottom of the pier occurred (squared markers in Fig. 3a) leading to the formation of an instable system. Further deformation of the structure led to reduction in cross-section of the piers (Figs. 4a and 5b). This extensive damage in the wide piers triggered local out-of-plane deformation of the
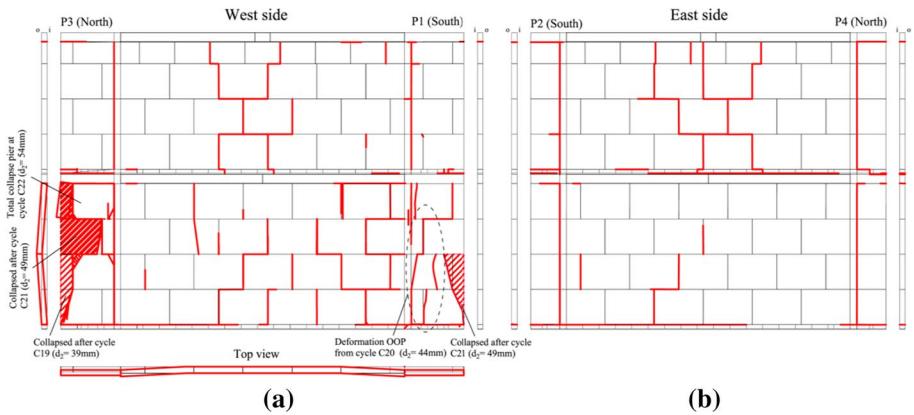
Fig. 4 Crack pattern after the last cycle ($d_2 = \pm 54$ mm): **a** West side; **b** East side. The drawings show the outside view of the structure. The reported damage is recorded by visual inspection carried out after each cycle. For sake of clarity, the piers are drawn on the same plane of the transversal walls (outside view)
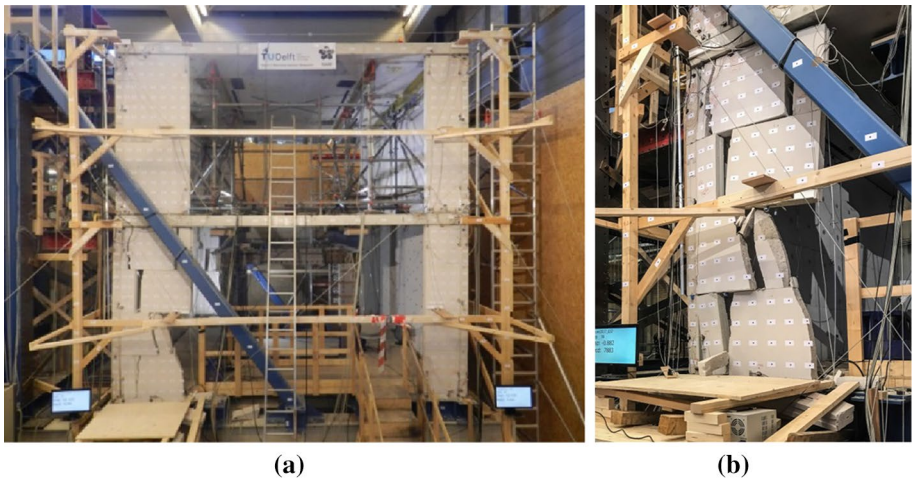
Fig. 5 Picture of the damaged assemblage in the last cycle ($d_2 = \pm 54$ mm): **a** entire structure in the first run (just before collapse of pier P3); **b** wide pier P1 at the end of the cycle

transversal wall on the west side (Fig. 4a) consequence of a wedge effect caused by the falling of masonry debris within the vertical joints (Puente et al. 2018). In the second run of the last cycle ($d_2 = \pm 54$ mm), full collapse of pier P3 occurred and severe damage in pier P1 was observed (Fig. 5b), while the rest of the structure appeared intact (Figs. 4 and 5b). The collapse of the wide piers at ground floor was considered as near collapse state, although the test could be continued. The progressive damage within the wider piers at the ground floor triggered a soft storey mechanism, resulting in an increase of inter-storey drift for the ground floor while the first floor showed a nearly constant value
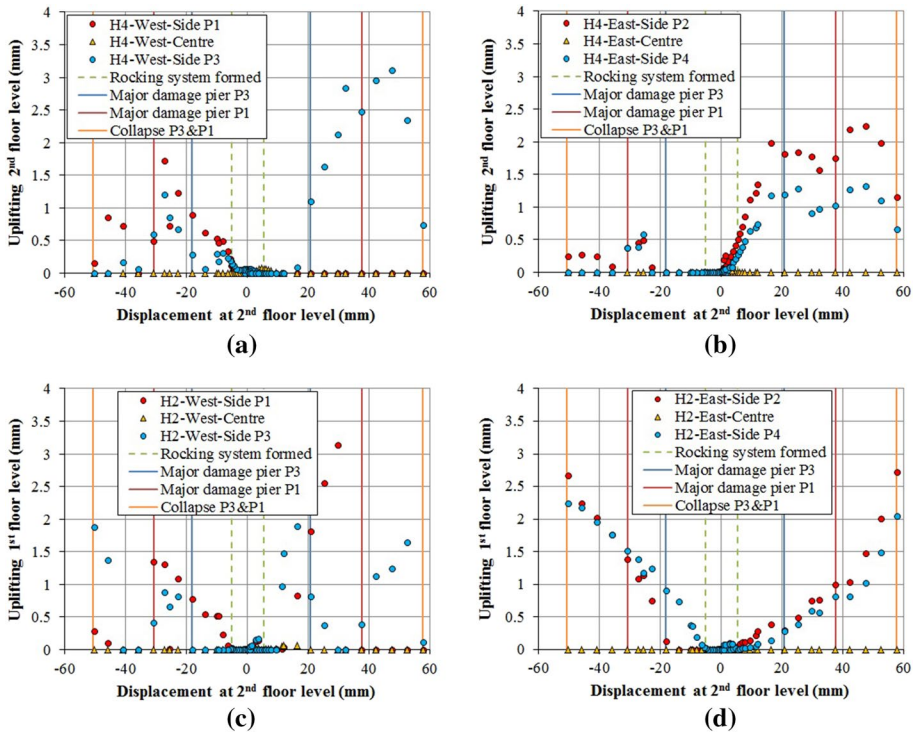
Fig. 6 Floor uplifting triggered by the rocking of the piers : **a–c** West wall; **b–d** East wall

(Fig. 3c). A maximum inter-storey drift of − 1.7 and + 1.8% is observed at ground floor for the negative and positive loading direction, respectively.

Although the quasi-static test discharges any inertial effects, and therefore not allows for a proper assessment of the local out-of-plane failure of the transversal walls, few observations can still be made. In presence of a real seismic event, the out-of-plane collapse could cause a premature failure of the structure that does not allow the development of the full in-plane displacement capacity of the piers (e.g. before damage in the wide pier starts). In this regard, the rocking of the piers as rigid blocks can induce the uplift of the floor promoting a change of top boundary conditions for the transversal wall and consequent risk of their out-of-plane failure. Figure 6 shows the floor uplift at first and second floor level. To determine the floor uplift, the crack opening of the horizontal joint between the transversal wall and the floor slab has been measured both on the inside and the outside of the structure. For each joint, three locations have been considered: one at the centre of the transversal wall and two in the proximity of the piers. For each location, the floor uplift was calculated as the minimum crack opening measured on the inside and the outside of the structure. A zero value of the floor uplift means that the floor and the transversal wall were still in contact (e.g. crack open on the outside of the structure, but close on the inside). In the graphs, average values for the three runs per cycles are considered for the crack opening values used to calculate the floor uplift and for the displacement at second floor level. For both the west and east wall, the rocking of the piers led to a floor uplift of approximately 3 mm, while in the centre the transversal wall was always in contact with the floor. At first

floor level the same trend is observed for positive and negative loading direction, while at second floor level larger values are observed for the positive loading direction. Being this a local phenomenon compatible with elastic deformation of the floor, it is reasonable to assume that throughout the test the top boundary conditions of the transversal walls were nearly unchanged. Considering that two-way spanning transversal walls can have a significant lateral resistance, it is expected that the floor uplift caused by the rocking of the piers is not sufficient to cause their out-of-plane failure before the full development of the in-plane capacity of façade piers. Different conclusions can be drawn in the case of similar structures subject to dynamic loading including vertical excitation (Tomassetti et al. 2018).

4 Seismic performance

In this section the seismic performance of the tested structure are analysed in terms of damage levels, bi-linearized capacity curve and hysteretic damping as support for the global seismic assessment.

Damage levels were defined on the basis of the experimentally observed damage and they are associated to the normalised base shear force ($k_G = V/V_{max}$), the inter-storey drift at ground floor d_{r1}, and the global drift d_r^*. The global drift has been calculated, similarly to Graziotti et al. (2017), as the ratio between the displacement at the second floor level and the total height of the specimen (5425 mm). A similar work has been carried out at single component scale (i.e. pier) for the near collapse (NC) limit state by Messali and Rots (2018). Table 2 and Fig. 7 show the obtained results and a comparison with the work presented by Lagomarsino and Cattari (2015), and by Graziotti et al. (2017); a representation of the damage levels on the backbone curve is shown in Fig. 8a. The damage level DL1, no visible damage, was identified with the last cycle before damage was observed at top and bottom of the piers. The damage level DL2, minor damage, was defined after the formation of the first minor damage in pier P3, namely opening of head joints and sliding on bed joints at the centre of the pier. The damage level DL3, moderate structural damage, was identified in correspondence of the formation of the first stepwise crack within the wide piers. The damage level DL4, corresponding to the NC state for which extensive (non-economically repairable) structural damage was observed, was associated to the formation of splitting cracks in the wide piers at the ground floor. By comparing the results with the values proposed by Lagomarsino and Cattari (2015), a good agreement is obtained for the first two damage levels, while for DL3 and DL4 larger value of inter-storey drifts and normalised base shear force reduction are obtained. This difference can be justified by the specific characteristics of the tested specimen (slender piers, absence of spandrels), which further promoted the development of the rocking mechanism of the piers. On the contrary, the work by Lagomarsino and Cattari (2015) dealt with a much wider category of heritage masonry structures that are often characterised by less ductile shear mechanisms. Additionally, the results are compared with the one obtained from the shaking table test performed by Graziotti et al. (2017) on a specimen resembling a brick masonry terraced house similar to the one presented in this paper. A good agreement is obtained in the identification of damage level DL1, but a discrepancy is observed for the other damage levels, in particular in terms of drift values, which results larger in the case of the structure presented in this work. The difference is reduced if the comparison is made in terms of global drift rather than the inter-storey drift at ground floor, confirming that the global response of the structure was governed by a similar failure mechanism, namely the rocking of the façade

Table 2 Identification of damage levels and comparison with the values proposed by Lagomarsino and Cattari (2015) and obtained by Graziotti et al. (2017)

Damage level	Tested specimen				Lagomarsino and Cattari (2015)		Graziotti et al. (2017)		
	Observed damage in the test	k_G	d_{r1}	d_r^*	k_G	d_r	k_G	d_r	d_r^*
		–	%	%	–	%	–	%	%
DL1	No observed damage.	0.55	−0.05	−0.04	>0.50	0.05–0.10	0.57	0.07	0.047
		0.66	0.02	0.04					
DL2	Minor damage. Opening head joints and sliding bed joints in wide pier P3.	0.99	−0.27	−0.18	0.95–1.00	0.15–0.30	0.76	0.12	0.073
		0.97	0.14	0.21					
DL3	Moderate and repairable structural damage. Stepwise cracks in the wide piers.	0.75	−0.74	−0.47	0.90–0.80	0.35–0.50	1.00	0.34	0.23
		0.85	0.66	0.59					
DL4	Extensive damage, not economically sustainable. Splitting of CS elements in wide piers and formation of instable mechanism.	0.58	−1.77	−0.93	0.60–0.70	0.55–0.70	0.66	0.88	0.73
		0.56	1.68	1.06					
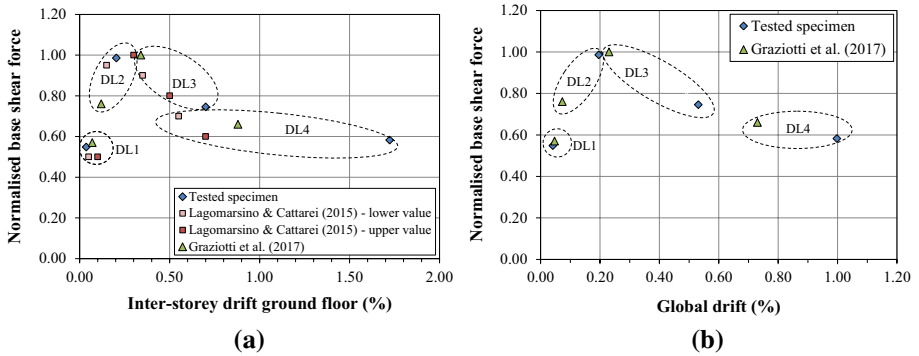
Fig. 7 Comparison in terms of damage levels with the values proposed by Lagomarsino and Cattari (2015) and obtained by Graziotti et al. (2017) considering: **a** inter-storey drift at ground floor; **b** global drift. Please note that for the tested specimen, the average value of the drift is reported for each damage level
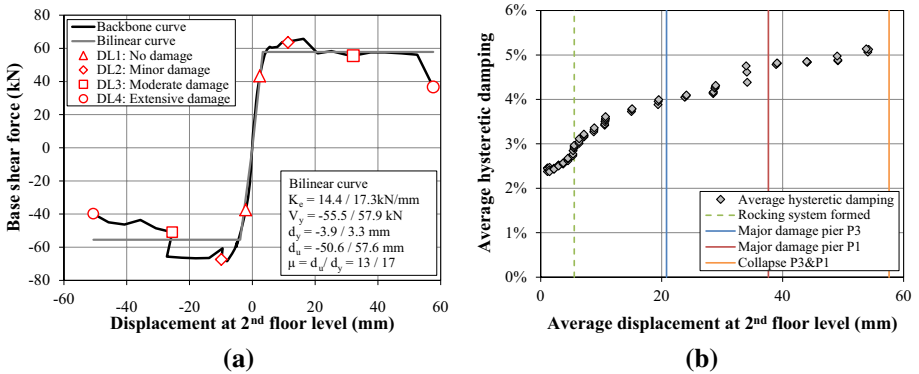
Fig. 8 **a** Identification of damage level and bilinear curve; **b** average hysteretic damping

piers. It should be noted that, differently than the presented case, the specimen tested by Graziotti et al. (2017) was composed also of a veneer wall and a timber roof in addition to the loadbearing structure. The near collapse state was identified, and the test consequently stopped, precisely as a consequence of the extensive deformation of these additional elements. Although dynamic effects are not considered in the quasi-static test presented in this paper, the comparison with the aforementioned shaking table test may then suggest that a substantial improvement of the global response of the structure can be obtained by preventing the local failure mechanisms of veneer and gable walls.

Within the perspective of a seismic assessment, the bi-linearization of the backbone curve is often required to determine the capacity of the structure. The obtained bilinear curve and the related parameters have been obtained separately for the negative and positive loading direction and are shown in Fig. 8a. The initial stiffness K_e of the bilinear curve was computed for a base shear equal to 70% of the maximum value obtained, as recommended in the Italian standards (MIT 2008). The ultimate displacement d_u was assumed in correspondence of the near collapse state, which is defined at damage level DL4. The peak force of the bilinear curve V_y was defined by imposing the equivalence in dissipated energy for the bilinear and the backbone curve. Considering the ratio between the ultimate

displacement d_u and the peak displacement d_y, the structure shows a ductility μ of 13 and 17 for the negative and positive loading direction, respectively.

To estimate the resistance to earthquakes in term of energy dissipation due to frictional mechanisms in the damaged state, an estimation of the hysteretic damping can be obtained from the quasi-static cyclic test. By considering the formulation first introduced by Jacobsen (1960) and reported by Priestley et al. (2007), the average hysteretic damping has been calculated considering the area within one complete run of stabilized force–displacement response. Figure 8b gives the average hysteretic damping as a function of the average displacement at second floor level, which has been calculated per each run considering the absolute maximum value of the displacement in positive and negative loading direction. To exclude the influence of possible friction in the actuators for low displacement, the value of hysteretic damping for displacements lower than 1 mm have been excluded. On average the hysteretic damping for the studied structure range between 3 and 5%.

5 Global seismic assessment

By using nonlinear static analysis procedure to assess the seismic vulnerability of masonry structures, the structural capacity is derived independently of the seismic demand requiring the use of an assessment procedure. Once the location of the structure is defined, and hence the corresponding hazard expressed in terms of acceleration–displacement response spectrum (ADRS), an assessment procedure is then needed to determine the seismic demand for each specific structure.

In this framework, the experimental results obtained from the quasi-static cyclic test are considered representative of the structural capacity and they are adopted to perform a global assessment. A representative location in the town of Loppersum (53.33N; 6.75E), situated in the area where the strongest earthquakes were recorded, has been selected. The elastic seismic response spectrum and the related elastic ADRS curve were derived on the basis of the Uniform Hazard Spectrum (UHS) currently provided by the Webtool NPR 9998 (NEN 2017a) and part of the new standard for seismic assessment NPR 9998:2018 (NEN 2018). The current hazard map has been derived on the basis of probabilistic studies and can be subject to modification in the future.[1] Currently, the expected maximum peak ground acceleration (PGA) is approximatively 4 times (PGA = 0.32 g) the recorded one (PGA = 0.08 g). This large difference does not allow studying the performance of Dutch terraced houses in situ, where the damage is limited, but it requires experimental tests as the one presented in this paper.

Three commonly used assessment procedures are considered: the capacity spectrum method (CSM) (ATC 1996), the N2 method (Fajfar 1999) and the recent alternative formulation of the N2 method for short-period structures proposed by Guerrini et al. (2017). The CSM method, initially developed for reinforced concrete structures, is based on the use of an overdamped spectrum determined via the estimate of an equivalent viscous damping related to the hysteretic capacity of the system. The N2 methods reduce the elastic spectrum using a behaviour factor R, that is computed differently for the general N2 method and its recent alternative formulation. Since the three methods account for the

---

[1] Please note that the paper was originally prepared on the basis of the hazard map retrieved on 9 April 2018, which is based on the version 4 of the ground motion model (GMM). In December 2018, an update of the hazard map was made based on the version 5 of GMM.

dynamic effects in a different manner, differences in the safety assessment can arise. For all method, the 'substitute structure' concept for the definition of the equivalent single degree of freedom (SDOF) system was adopted as proposed by Magenes and Calvi (1997) for masonry structures. To define the capacity curve of the equivalent SDOF system, an effective mass equal to the total mass of the structure (36.9 t) was considered without any load factor. A unit participation factor Γ was assumed as assumed by Causevic and Mitrovic (2011) when uniform loading distribution is applied to the structure and in accordance with the recommendations of Appendix B in EN 1998-1 (CEN 2005). This represents in fact a small approximation of the real behaviour of the structure, since a failure mechanism close to a soft storey mechanism (especially in the negative loading direction) was observed. It should be noted that a standard safety assessment of the structure would consider in addition other load distributions, as well as torsional effects and accidental eccentricity; these effects are here neglected because they were not object of the presented experiment. The displacement capacity at near collapse was computed as the maximum lateral displacement at second floor level measured during the test, in accordance with the damage level DL4 defined in Table 2. Unlike the CSM, the N2 methods require also a bi-linearization of the capacity curve for the idealised equivalent SDOF system (Fig. 8a), which parameters are defined in Table 3 in terms of period T^*, peak spectral acceleration $S_{a;y}$ and NC spectral displacement $S_{d;NC}$. In the case of the CSM, it is required to define an overdamped ADRS curve. This curve is derived by multiplying the elastic ADRS spectrum by a spectral reduction factor η_ξ, function of the effective equivalent viscous damping ξ_{sys} of the structure. The value ξ_{sys} is defined in NPR 9998:2018 (NEN 2018), and includes a lumped contribution attributable to the soil-structure interaction ($\xi_{soil} = 10\%$), along with the inherent damping (ξ_{el}, usually estimated equal to 5%) and the hysteretic damping ξ_{hys}. In NPR 9998:2018 a hysteretic damping value $\xi_{hys} = 15\%$ is recommended for structures with ductility μ larger than 4. Considering that the tested specimen has a low energy absorption (Priestley et al. 2007), the assessment is also performed adopting the hysteretic damping obtained from the experiment (Fig. 8b) considering a displacement at second floor level equal to the target displacement. As a consequence, two different overdamped ADRS curves are considered: one based on the recommendations of the standard ($\xi_{sys} = 30\%$) and the other consistent with the hysteretic damping derived by the experimental test ($\xi_{sys} = \xi_{el} + \xi_{soil} + \xi_{hyst} \approx 5\% + 10\% + 5\% = 20\%$).

For the standard N2 method, the target displacement was determined according to the procedure described in the informative Annex B of EN 1998—part 1 (CEN 2005). The structure is verified for the selected location only if the ratio between the NC displacement (capacity) and the target displacement (demand) is larger than the unity (C/D > 1). The alternative formulation of the N2 method for short-period structures adopts the same procedures described for the standard N2 method, but it proposes a different equation to compute the inelastic target displacement that includes additional parameters properly calibrated for the response of short-period masonry structures (Guerrini et al. 2017). In this paper, the values recommended for flexure-dominated structures are used ($a_{hyst} = 0.7$, $b = 2.3$, $c = 2.1$, and $T_{hyst} = 0.055$).

The relevant parameters used for the seismic assessment according to the three abovementioned procedures are listed in Table 3, while Table 4 shows the obtained results in terms of C/D ratios; a graphical interpretation of the assessment is shown in Fig. 9. As regards the CSM, the value of the hysteretic damping suggested in NPR 9998:2018 is larger than the one derived from the experimental test. However, it should be mentioned that the Dutch guidelines consider the contribution to damping of every structural and nonstructural component of a building other than the loadbearing structure. The difference

Table 3 Significant parameters used for the seismic assessment of the tested structure

Loading direction	T^*	$S_{a;y}$	$S_{d;NC}$	R	$\eta_{\xi;NPR}$	$\eta_{\xi;exp}$	d^*_{et}	$d^*_{t;N2}$	$d^*_{t;N2-mod}$	$d^*_{t;CSM-NPR}$	$d^*_{t;CSM-exp}$
	s	g	mm	–	–	–	mm	mm	mm	mm	mm
Negative	0.32	0.153	50.6	3.48	0.467	0.565	13.44	22.46	31.87	37.20	46.54
Positive	0.29	0.160	57.6	3.34	–	–	11.18	20.03	30.20	35.25	44.36

T^*: period of the idealized SDOF system; $S_{a;y}$: peak spectral acceleration; $S_{d;NC}$: NC spectral displacement; R: strength reduction factor; $\eta_{\xi;NPR}$ and $\eta_{\xi;exp}$: spectral reduction factors computed using a damping value based on NPR 9998:2018 recommendations and experimental outcomes, respectively; d^*_{et}: elastic target displacement; $d^*_{t;N2}$ and $d^*_{t;N2-mod}$: target displacements for the N2 method and the short-period structures N2 method, respectively; $d^*_{t;CSM-NPR}$ and $d^*_{t;CSM-exp}$: target displacements for the CSM method computed using the spectral reduction factors $\eta_{\xi;NPR}$ and $\eta_{\xi;exp}$, respectively

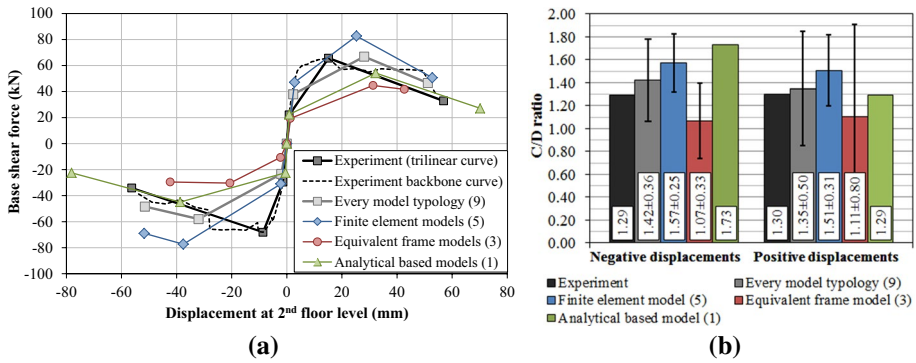**Table 4** Seismic assessment of the tested structure for near collapse according to different assessment procedures

Return period	Assessment procedure	Capacity over demand ratio (C/D)	
Years		Negative loading	Positive loading
2475	CSM (NPR damping)	1.36	1.63
2475	CSM (experimental damping)	1.09	1.30
2475	N2 method	2.25	2.88
2475	Short-period structures N2 method	1.59	1.91
95	CSM (elastic ADRS)	11.40	15.03
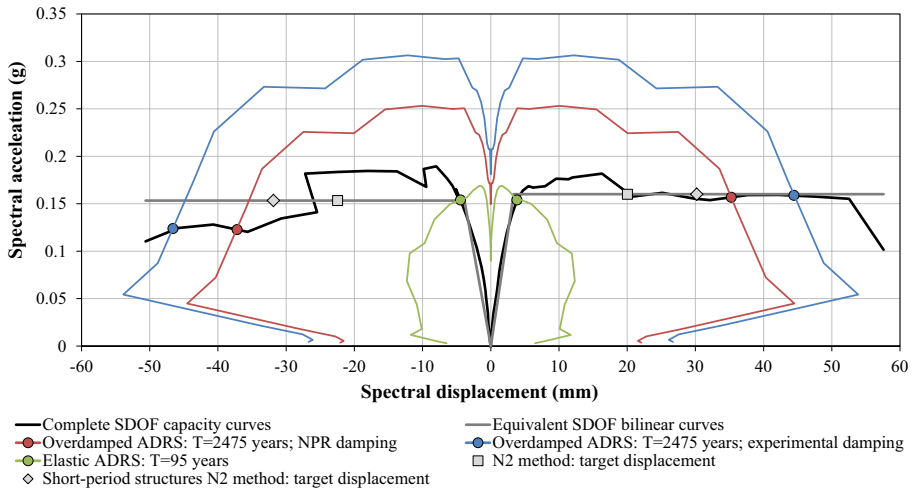
Fig. 9 Comparison between the SDOF capacity curves and the demand defined according to different assessment procedures. The figure includes the capacity and demand curves for both positive and negative spectral displacements. Absolute spectral accelerations are considered

between the two computed overdamped curves is anyhow rather limited, and it does not change the results of the assessment. The general N2 method is characterised by significantly smaller demands (and, hence, larger C/D ratios). This detail is emended by the alternative N2 method proposed by Guerrini et al. (2017) that was derived specifically for URM buildings, whose C/D ratios are closer to those predicted by the CSM. In general, the studied structure would be verified in the selected location for each of the three considered assessment procedures, but significantly different C/D ratios are obtained. Consequently, the selection of the method is confirmed to be of high relevance.

Being the recorded earthquake magnitude lower than the maximum expected value currently incorporated in the hazard map, the assessment is performed also considering the largest recorded magnitude (PGA = 0.08 g). The displacement demand has been defined using the elastic ADRS curve corresponding to a return period of 95 years in location previously considered (green curve in Fig. 9). The assessment is performed according to the CSM, but similar results would be achieved with any other method, since the structure has almost an elastic response for the considered demand. The obtained target displacement

Fig. 10 Comparison between experimental and predicted averaged results for analysis typology: **a** simplified capacity curve of the structure; **b** seismic assessment of the tested structure according to the CSM. The number of participants using the modelling approach is given in brackets

corresponds to the formation of the rocking mechanism, when cracks were observed at top and bottom of the piers, and at the vertical joints between piers and transversal walls. This limited damage is in line with preliminary observations of damage in existing buildings (ARUP 2013) and it is consistent with the large C/D ratios obtained (Table 4). Consequently, beside the assessment at near collapse, the damage assessment for the actual recorded earthquakes is of importance (Korswagen et al. 2018).

6 Assessment from engineering practice: blind prediction contest results

The assessment described in Sect. 5 makes use of the experimental capacity curve; however, few experimental tests at full-scale are available, and the assessment performed by engineering companies is often based on the outcomes of numerical analyses or analytical computations. The use of different modelling approaches usually leads to different predictions, being some models more suitable than others for specific masonry and building typologies (Giamundo et al. 2014). The differences are even larger when different users are asked to simulate the nonlinear behaviour of a structure (Mendes et al. 2017). For this reason, the quasi-static cyclic test was selected for a blind prediction contest (Messali et al. 2018b) with the primary aim of (i) sharing the knowledge between consultancy firms, (ii) improving the understanding of the structural behaviour of a typical URM structure, and (iii) contributing to the development of the Dutch guidelines for the seismic assessment of existing buildings (NEN 2017b, 2018). Nine engineering companies working for the seismic assessment of the Groningen building stock participated to the contest. Different modelling approaches, type of structural analysis and assessment criteria were adopted to predict the behaviour of the tested structure. Mean measured material properties were provided to the participants.

The received predictions can be categorised in three groups, according to the adopted modelling strategy: five finite element (FE) models; three equivalent frame (EF) models, and one analytical-based model. Even though the dispersion of the results is rather high within each of these groups, some trends can be synthetically outlined with the support of Fig. 10a, which shows simplified averaged curves for each group, derived considering

the onset of cracking, the peak, and the near collapse. All the predictions properly identified the rocking mechanism of the structure at failure; however, only four models could accurately describe the collapse of the wide piers at ground floor. The damage evolution in the wide piers P1 and P3, with the development of splitting diagonal cracks that eventually led to the partial collapse of the structure, could not be identified by EF models, whose analyses only showed the initial activation of the rocking mechanism, while it was correctly represented by few FE models, which usually can better capture the evolution of a failure mechanism; on the other hand, the analytical-based model provided a rough but in fact correct description of the collapse mechanism. This suggests that even complex failure modes can be satisfactorily described by simple analytical methods when the geometry of the structure is simple enough, such as in the considered case, as observed also for other simple rocking systems (Sarhosis et al. 2018). In terms of evaluation of the force and displacement capacity of the structure, the predictions based on FE models were characterised by a small overestimation of the peak strength and a slight underestimation of the ultimate displacement capacity. On the opposite, the analytical-based model underestimated the capacity in terms of forces, but it overestimated the displacement capacity of the structure. Finally, the analyses based on EF models generally underestimated the experimental capacity in terms of both force (at peak load) and displacement (at near collapse). Overall, given the highlighted trends, the combination of different approaches allows for a better understanding of the modelled structural behaviour. Specifically, simple hand calculation based on analytical models prevent from overlooking and incorrect modelling choices in more complex FE analyses.

To assess the capacity of the structure as an engineering company would do in practice, the procedure described in Sect. 5 was repeated considering the capacity curves and the ultimate displacement as submitted by the companies. The assessment procedure recommended in the NPR 9998:2018 (NEN 2018) was considered (CSM, $\xi_{sys} = 30\%$). Figure 10b gives an overview of the assessment results. The result of the assessment of a structure depends mainly on the combination of the displacement and the residual force at near collapse. The abovementioned underestimation of both strength and displacement capacity given by EF models resulted on average in smaller values of C/D ratios, even though larger than one (i.e. the structure would be verified). On the contrary, when the assessment procedure was performed by either finite element or analytical based analyses the obtained C/D ratios were on average larger than those computed for the experiment. Overall, the C/D ratio computed as average of every simulation was close to that derived from the experimental values, but a large dispersion of the results was observed (Fig. 10b).

7 Concluding remarks

Mainly designed according to wind-resistant criteria, terraced houses have characteristics that can limit their seismic performance such as presence of narrow piers, cavity walls, slender walls and weak connections between structural elements. They are one of the most present typology among unreinforced masonry (URM) buildings in the Groningen region (the Netherlands), where recently the exploitation of geo-resources is triggering shallow earthquakes. Consequently, their seismic assessment become of importance.

In this framework, a quasi-static cyclic test has been carried out at Delft University of Technology on a calcium silicate (CS) element masonry assemblage resembling a typical modern Dutch terraced house built after 1980 and still commonly used nowadays.

The full-scale two-storey specimen, representing only the inner loadbearing structure of a terraced house, was composed of two identical facades having each a wide pier and a narrow pier. The floors, made of pre-fabricated reinforced concrete, were one-way spanning between the transversal walls. Mortar joints were used for the wall/pier-to-floor and the wall-to-pier connections. In the latter case, steel ties embedded at every mortar joint between masonry elements were also used.

The test aimed at investigating the response of the structure laterally loaded along the façade piers, being this the most vulnerable direction for the global seismic behaviour of the structure. By performing a quasi-static cyclic test, the structural behaviour was mainly related to the in-plane response of the façade piers; premature failure of transversal walls due to dynamic effects were thus not considered in the test. Although two pier sizes were used in the façade, the structural response was mainly governed by the behaviour of the wide piers at the ground floor. The test was carried out up to the full collapse of those piers, reaching an inter-storey drift of approximately $\pm 1.7\%$ at ground floor. Due to the large size of the masonry units, the wide piers showed first rocking behaviour as a rigid block followed by a brittle splitting failure causing failure of the piers. The rocking of the piers caused a local uplift of the floors, which however did not released substantially the top support of the transversal walls. Throughout the test the transversal walls accommodate the in-plane deformation of the façade piers, although cracking at the vertical joint connecting them occurred approximately at the peak load; the coupling was maintained thanks to the presence of the steel ties (embedded in the bed joints) and the sliding friction mechanism at the vertical joint.

To evaluate the seismic performance of the tested structure, four damage levels were identified, namely DL1 no visible damage, DL2 minor damage, DL3 moderate structural damage, DL4 extensive structural damage whom repair is not economical. The damage levels were defined on the basis of the observed crack pattern and they are expressed in terms of normalised base shear force and inter-storey drift at ground floor. By comparing those values with literature information, a good agreement can be observed for the normalised base shear force. Differently, the experimental inter-storey drift results higher than value commonly reported in literatures; this can be related to the ductile rocking mechanisms of the piers and the absence of spandrels as well as to the absence of secondary elements such as veneer and gable walls that may be more vulnerable to premature failure.

Various assessment procedures were adopted in the framework of the nonlinear static analyses by considering the experimental results as representative of a typical building in the Groningen area. The assessment was carried out considering the capacity spectrum method (CSM), the N2 method and an alternative N2 method suitable specifically for short-period masonry structures. A location with the highest seismic demand (PGA = 0.32 g), as predicted by the current hazard map, was selected. For the presented case, the structure is verified in the selected location for each of the three considered assessment procedures, but significantly different C/D ratios are computed. The choice of the assessment procedure is hence confirmed to be of high relevance.

For a qualitative comparison in terms of damage, the seismic response of the structure has been considered also with respect to the highest recorded seismic demand in the region up to now (PGA = 0.08 g). In this case, the required target displacement corresponded to the one that experimentally led to the formation of the rocking mechanism (only cracks at the wall/pier-to-floor connections). This limited damage is in line with preliminary observations of damage in existing buildings and it is consistent with the large C/D ratios obtained.

Considering that the validation of analysis method used in engineering practice is of high relevance, the presented case study has been used as a benchmark in a blind prediction contest involving nine engineering consultancy firms working for the seismic assessment of the Groningen building stock. The participants adopted different methods, namely finite element method, equivalent frame approach and analytical calculations. In all cases a large variability in the prediction of both force and displacement capacity was observed. The combination of more than one approach allows to compare and cross-validate the results and to provide more accurate predictions.

The present study is a step forward to assess the seismic vulnerability of Dutch terraced houses. Being this typology of building design only as a wind-resistant system, its specific characteristics rose doubts on their ability to withstand seismic loads. In the case of the tested structure, the global capacity was larger than the maximum seismic demand expected according to the current hazard map. Such a conclusion, derived for the specific conditions of the experimental test, does not have a general validity, and other studies, including statistical approaches, are needed to assess the seismic vulnerability of the whole population of terraced houses. In this framework, the presented experimental results represent an important benchmark for the validation of analysis methods.

8 Access to experimental data

The experimental results of the presented test are available via the repository 4TU. ResearchData at http://doi.org/10.4121/uuid:9b52a971-6cd3-402e-a496-81d01e32604e. The data are distributed under the license type CC BY.

References

Aldemir A, Binici B, Canbay E, Yakut A (2017) Lateral load testing of an existing two story masonry building up to near collapse. Bull Earthq Eng 15(8):3365–3383

Anthoine A, Capéran P (2008) ESECMaSe—D 8.3 Earthquake tests and analysis of the experimental results. European Laboratory for Structural Assessment (ELSA), Joint Research Centre of the European Commission, Ispra

ARUP (2013) Groningen 2013—structural upgrading study. REP/229746/SU003, ARUP, Amsterdam

ATC (1996) ATC-40 Seismic evaluation and retrofit of concrete buildings. Redwood City, Applied Technology Council

Bourne S, Oates S, Bommer J, Dost B, Van Elk J, Doornhof D (2015) A Monte Carlo method for probabilistic hazard assessment of induced seismicity due to conventional natural gas production. Bull Seismol Soc Am 105(3):1721–1738

Calvi GM, Kingsley GR, Magenes G (1996) Testing of masonry structures for seismic assessment. Earthq Spectra 12(1):145–161

Causevic M, Mitrovic S (2011) Comparison between non-linear dynamic and static seismic analysis of structures according to European and US provisions. Bull Earthq Eng 9(2):467–489

CEN (1998) EN 1052-1—method of test masonry—part 2: determination of compressive strength. European Committee for Standardisation, Brussels

CEN (1999) EN 1015-11—method of test for mortar for masonry—part 11: determination of flexural strength of hardened mortar. European Committee for Standardisation, Brussels

CEN (2000) EN 772-1—methods of test for masonry units—part 1: determination of compressive strength. European Committee for Standardisation, Brussels

CEN (2002) EN 1052-3—method of test masonry—part 3: determination of initial shear strength. European Committee for Standardisation, Brussels

CEN (2005) EN 1998–1—Eurocode 8: design of structures for earthquake resistance—part 1: general rules, seismic actions and rules for buildings. European Committee for Standardisation, Brussels

CEN (2009) EN 12390-3—testing hardened concrete—part 3: compressive strength of test specimens. European Committee for Standardisation, Brussels

CEN (2015) EN 1052-2—method of test masonry—part 2: determination of flexural strength. European Committee for Standardisation, Brussels

Damiola M, Esposito R, Messali F, Rots J (2018) Quasi-static cyclic two-way out-of-plane bending tests and analytical models comparison for URM walls. In: Milani G, Taliercio A, Garrity S (eds) 10th international masonry conference (IMC). Milan, Italy

Degée H, Denoël V, Candeias P, Campos Costa A, Coelho E (2008) Experimental investigations on non-engineered masonry houses in low to moderate seismicity areas. In: Proceedings of the 14WCEE, 14th world conference on earthquake engineering

Esposito R, Messali F, Rots JG (2016) Tests for the characterization of replicated masonry and wall ties. Delft University of Technology, Delft

Esposito R, Jafari S, Ravenshorst GJP, Schipper HR, Rots JG (2018) Influence of the behaviour of calcium silicate brick and element masonry on the lateral capacity of structures. In: 10th Australasian masonry conference, Sydney

Fajfar P (1999) Capacity spectrum method based on inelastic demand spectra. Earthq Eng Struct Dyn 28:979–993

Giamundo V, Sarhosis V, Lignola G, Sheng Y, Manfredi G (2014) Evaluation of different computational modelling strategies for the analysis of low strength masonry structures. Eng Struct 73:160–169

Graziotti F et al (2015) Experimental campaign on cavity-wall systems representative of the Groningen building stock. Report No. EUC318/2015U, EUCENTRE, Pavia, Italy

Graziotti F, Tomassetti U, Kallioras S, Penna A, Magenes G (2017) Shaking table test on a full scale URM cavity wall building. Bull Earthq Eng 15(12):5329–5364

Graziotti F, Penna A, Magenes G (2018) A comprehensive in situ and laboratory testing programme supporting seismic risk analysis of URM buildings subjected to induced earthquakes. Bull Earthq Eng. https://doi.org/10.1007/s10518-018-0478-6

Guerrini G, Graziotti F, Penna A, Magenes G (2017) Improved evaluation of inelastic displacement demands for short-period masonry structures. Earthq Eng Struct Dyn 46(9):1411–1430

Jacobsen LS (1960). Damping in composite structures. In: 2nd world conference on earthquake engineering (WCEE), vol 2, pp 1029–1044, Tokyo and Kyoto, Japan

Jafari S, Esposito R (2017) Material tests for the characterisation of replicated calcium silicate element masonry. C31B67WP1-11, Delft University of Technology

Jafari S, Esposito R, Rots JG (2018) From brick to element: investigating the mechanical properties of calcium silicate masonry. In: 11th international conference on Structural Analysis of Historical Constructions (SAHC). Cusco, Peru

Korswagen PA, Longo M, Meulman E, Rots JG (2018) Crack initiation and propagation in unreinforced masonry specimens subjected to repeated in-plane loading during light damage. Bull Earthq Eng. https://doi.org/10.1007/s10518-018-00553-5

Lagomarsino S, Cattari S (2015) PERPETUATE guidelines for seismic performance-based assessment of cultural heritage masonry structures. Bull Earthq Eng 13(1):13–47

Magenes G, Calvi GM (1997) In-plane seismic response of brick masonry walls. Earthq Eng Struct Dyn 26(11):1091–1112

Magenes G, Calvi GM, Kingsley GR (1995) Seismic testing of a full-scale, two-story masonry building: test procedure and measured experimental response. In: Experimental and numerical investigation on a brick masonry building prototype—numerical prediction of the experiment, Report 3.0—G.N.D.T. Eds., University of Pavia, Department of Structural Mechanics, pp 1.1–1.41

Mayer U, Caballero Gonzaléz A (2008) ESECMaSE—shaking table tests at the national technical university in Athens. In: 14th international brick and block masonry conference, Sydney

Mendes N et al (2017) Methods and approaches for blind test predictions of out-of-plane behavior of masonry walls: a numerical comparative study. Int J Archit Heritage 11(1):59–71

Messali F, Rots JG (2018) In-plane drift capacity at near collapse of rocking unreinforced calcium silicate and clay masonry piers. Eng Struct 164:183–194

Messali F, Esposito R, Jafari S, Ravenshorst GJP, Korswagen P, Rots JG (2018a) A multiscale experimental characterisation of Dutch unreinforced masonry buildings. In: 16th European Conference on Earthquake Engineering (ECEE), Thessaloniki

Messali F, Pari M, Esposito R, Rots JG (2018b) Blind prediction of a cyclic pushover test on a two-storey masonry assemblage: a comparative study. In: 16th European Conference on Earthquake Engineering (ECEE), Thessaloniki

NEN (2012) NPR 9096-1-1—masonry structures—simple design rules, based on NEN-EN 1996-1-1+C1. Nederlands Normalisatie-instituut, Delft

NEN (2017a) http://seismischekrachten.nen.nl/webtool.php. Retrieved 09 April 2018

NEN (2017b) NPR 9998—assessment of structural safety of buildings in case of erection, reconstruction and disapproval—basic rules for seismic actions: induced earthquakes. Nederlands Normalisatie-instituut, Delft

NEN (2018) NPR 9998—assessment of structural safety of buildings in case of erection, reconstruction and disapproval—induced earthquakes—basis of design, actions and resistances. Nederlands Normalisatie-instituut, Delft

Priestley MJN, Calvi GM, Kowalsky MJ (2007) Displacement-based seismic design of structures. IUSS Press, Pavia

Puente I, Lindenbergh R, van Natijne A, Esposito R, Schipper HR (2018) Monitoring of progressive damage in buildings using laser scan data. In: ISPRS technical commission II symposium 2018, Riva del Garda

Sarhosis V, Milani G, Formisano A, Fabbrocino F (2018) Evaluation of different approaches for the estimation of the seismic vulnerability of masonry towers. Bull Earthq Eng 16(3):1511–1545

Tomassetti U, Correia AA, Candeias PX, Graziotti F, Costa AC (2018) Two-way bending out-of-plane collapse of a full-scale URM building tested on a shake table. Bull Earthq Eng. https://doi.org/10.1007/s10518-018-0507-5

van Eck T, Goutbeek F, Haak H, Dost B (2006) Seismic hazard due to small-magnitude, shallow-source, induced earthquakes in The Netherlands. Eng Geol 87(1–2):105–121

van Elk J, Doornhof D (2017) Induced seismicity in Groningen. Assessment of hazard, building damage and risk. Nederlandse Aardolie Maatschappij B.V

Vlek C (2018) Induced earthquakes from long-term gas extraction in Groningen, the Netherlands: statistical analysis and prognosis for acceptable—risk regulation. Risk analysis

Yi T, Moon FL, Leon RT, Kahn LF (2006) Lateral load tests on a two-story unreinforced masonry building. J Struct Eng 132(5):643–652

Affiliations

Rita Esposito[1] · **Francesco Messali[1]** · **Geert J. P. Ravenshorst[2]** ·
H. Roel Schipper[1] · **Jan G. Rots[1]**

Francesco Messali
f.messali@tudelft.nl

Geert J. P. Ravenshorst
g.j.p.ravenshorst@tudelft.nl

H. Roel Schipper
h.r.schipper@tudelft.nl

Jan G. Rots
j.g.rots@tudelft.nl

1   Department of Materials, Mechanics, Management and Design, Delft University of Technology,
     Stevinweg 1, 2628 CN Delft, The Netherlands

2   Department of Engineering Structures, Delft University of Technology, Stevinweg 1,
     2628 CN Delft, The Netherlands